MESOSCALE ELASTIC CONSTANTS IN GRAPHITE

Gianluca Savini[1, 2] and Malcolm I Heggie[1]
[1]Dept of Chemistry, University of Sussex, Falmer, Brighton, BN1 9QJ, United Kingdom
[2]Dept of Physics, University of Bologna, Bologna, 40126, Italy

Abstract

First principles density functional calculations within the Local Density Approximation (LDA) have provided highly plausible results but the folklore of interlayer interactions is that LDA does not include an important part of the physical interaction between layers (dispersion forces *i.e.* van der Waals force) and therefore should not be relied upon. Contradicting this belief, we have demonstrated that LDA performs excellently for graphite and reproduces with precision all the elastic properties.

Introduction

Graphite, the prototypical-layered material consists of parallel sheets of atoms in the AB Bernal stacking sequence. The crystal structure is consistent with the D_{6h}^4 ($P6_3/mmc$) space group and has four carbon atoms per unit cells. The intralayer bonding is due to overlap between sp^2-hybridized orbital forming σ-bonds between nearest-neighbour C atoms. In addition, π-bonding takes place between the remaining p_z-orbitals on each atom that point perpendicularly to the layer; such π-electrons are delocalized throughout the layer so that individual single and double carbon bonds cannot be recognized. This highly anisotropic bonding characterized by exceptional strong sp^2 covalent intralayer bonding and weak interlayer bonding gives rise to a number of unusual properties that are of long-standing technological and scientific importance. Last but not least, there has been a resurgence of interest in graphite as a primary component of the graphite intercalation compounds formed by inserting various atoms or molecules between the loosely bonded layers of a graphite.

Several sources of crystalline graphite are available, but differ somewhat in their overall characteristics. Natural single crystal graphite flakes are usually small in size (typically much less than 0.1 mm in thickness), and contain defects in the form of twinning planes and screw dislocations. They also contain chemical impurities like transition metals. The most commonly used high-quality graphitic material today is Highly Orientated Pyrolytic Graphite (HOPG), which is prepared by the pyrolysis of hydrocarbons at temperatures above 2000°C and the resulting pyrolytic carbon is subsequently heat treated to higher temperature to improve its crystalline order. When stress annealed above 3300°C, the HOPG exhibits electronic, transport, thermal, and mechanical properties close to those of single-crystal graphite, showing a very high degree of *c*-axis alignment. This material is commonly used because of its good properties, high chemical purity, and relatively large sample sizes Kelly (1981), Dresselhaus *et al* (2000).

The elastic behaviour of a completely asymmetric material is specified by 21 independent elastic constants, while for isotropic material, the number is reduced to 2. In between these two limits, the necessary number is determined by the symmetry of the material. In case of hexagonal crystals (graphite), the number of the second-order elastic constants is 5.
The most complete experimental study on the graphite elastic constants is the work of Blakslee *et al* (1970). These authors have determined the full sets of second-order elastic constants by ultrasonic, sonic resonance and static test methods. The graphite samples used by Blakslee *et al* were turbostratic graphite (plane randomly oriented[1]).

These samples were annealed under a compressive stress perpendicular to the basal plane in order to promote the crystalline growth (up to 20 − 50 μm) and aligns within 0.1º − 0.5º along the *c*-axis. Among the five elastic constants found by Blakslee *et al*, two of them (C_{44}, C_{13}) have been revised Cousin *et al* (2003).

The reported value of C_{44} was lowered by the gliding of basal dislocations (the stress needed to move basal dislocations in graphite is quasi zero). Baker *et al* (1964) have shown that a light dose of neutron irradiation at relatively low-temperature pins the dislocations and thereby increase the C_{44} value up to 5.05± 0.35 GPa (see also Grimsditch (1996, 1983) and Lee *et al* (1990)). The latter result is the revised value of C_{44}.

A new value for C_{13} was proposed by Zhao *et al* (1989). In this work, *x*-ray diffraction data have been obtained on polycrystalline graphite and using the linear bulk modulus, these authors suggested a higher value of 22 ± 2 GPa. Unfortunately, they inadvertently used the expression for the planar bulk modulus and not the linear bulk modulus. If their procedure was carried through correctly, the value of C_{13} is lowered to 7.9 ± 3.5 GPa Cousin *et al* (2003). The latter elastic constant is the revised value for C_{13}.

[1] Because second-order elasticity is isotropic in the basal plane, the random plane orientations do not affect the second-order elastic constants Blakslee *et al* (1970). This isotropy does not extend to the third-order elastic constant Cousin *et al* (2003).

In Table 1 are resumed the second-order elastic constants measured using different experimental techniques (bottom side of the table) and calculated within the local density functional theory (top side of the table). The last row resumes the revised experimental elastic constants Cousin *et al* (2003) that are believed to be the most reliable. As I pointed out in the introduction, the value of the elastic constant C_{13} is positive for experimental studies and negative for theoretical studies.

Methods

The calculations are based on density functional theory in the local density approximation using the exchange-correlation functional as parameterized by Perdew and Wang (1992). Norm-conserving pseudopotentials with non-local core corrections based on the Hartwigsen-Goedecker-Hutter scheme (1998) were used. The charge density was represented by a plane-wave basis in reciprocal space expanded up to 2000 Ryd, while the Brillouin zone integrations were performed with a Monkhorst-Pack (1976) scheme with mesh up to 128 · 128 · 16 k-points. The basis sets employed consist of s, p and d Gaussian orbital functions with four exponents, centered at the atomic sites. Typical basis set used were pppp, pdpp, pddp, pdddp.

Here the elasticity of graphite was studied using the basis set pdpp, a *k*-points mesh of 16 · 16 · 6 and a charge density cut-off of 600 Ryd. Test calculations have shown that even if the total energy is 5 mRyd/atom higher than the convergence value (basis set pdddp, *k*-points mesh of 128 · 128 · 16, charge density cut-off of 2000 Ryd), the lattice parameters and respective elastic constants were still well convergent (due to cancellation of errors between energy differences). The lattice parameters found were $a = 2.444$ Å and $c = 6.63$ Å in good agreement with the respective experimental values $a = 2.452$ Å, $c = 6.67$ Å (Zhao *et al* (1989), Baskin *et al* (1955)).

The Classical Elastic Constants

Under small deformations, the elastic energy of a crystal can be expressed as a Taylor expansion in terms of the strain components (Landau and Lifshitz (1986)):

$$w = \frac{1}{2!}\sum_{i=1}^{6}\sum_{j=1}^{6} C_{ij}\varepsilon_i\varepsilon_j + \frac{1}{3!}\sum_{i=1}^{6}\sum_{j=1}^{6}\sum_{k=1}^{6} C_{ijk}\varepsilon_i\varepsilon_j\varepsilon_k \tag{1}$$

where w is the elastic energy per unit volume, C_{ij}, C_{ijk} are the second- and third-order elastic constants and ε_i are the strain components. For hexagonal crystals, we have 15 independent elastic constants, while the remaining constants are related to them by crystal symmetries. Therefore, the strain energy became:

$$\begin{aligned} w = {} & +\frac{1}{2}\left(\varepsilon_1^2+\varepsilon_2^2+\frac{1}{4}\varepsilon_6^2\right)C_{11}+\left(\varepsilon_1\varepsilon_2-\frac{1}{4}\varepsilon_6^2\right)C_{12}+\left(\varepsilon_1\varepsilon_3+\varepsilon_2\varepsilon_3\right)C_{13}+\frac{1}{2}\left(\varepsilon_3^2+\varepsilon_5^2\right)C_{44}+\frac{1}{6}\varepsilon_3^3C_{333}+ \\ & +\frac{1}{2}\left(\frac{1}{3}\varepsilon_1^3+\frac{1}{2}\varepsilon_1^2\varepsilon_2+\frac{1}{2}\varepsilon_1\varepsilon_2^2+\frac{1}{3}\varepsilon_2^3\right)C_{111}+\left(\frac{1}{2}\varepsilon_1^2\varepsilon_3+\varepsilon_1\varepsilon_2\varepsilon_3+\frac{1}{2}\varepsilon_2^2\varepsilon_3\right)C_{113}+\frac{1}{2}\left(\varepsilon_3\varepsilon_4^2+\varepsilon_3\varepsilon_5^2\right)C_{344}+ \\ & +\frac{1}{2}\left(-\varepsilon_1^2\varepsilon_2-2\varepsilon_1\varepsilon_2^2+\frac{1}{3}\varepsilon_2^3+\varepsilon_1\varepsilon_6^2\right)C_{166}+\frac{1}{2}\left(\varepsilon_1\varepsilon_4^2+\varepsilon_2\varepsilon_5^2-\varepsilon_4\varepsilon_5\varepsilon_6\right)C_{144}+\frac{1}{2}\left(\varepsilon_1\varepsilon_3^2+\varepsilon_2\varepsilon_3^2\right)C_{133}+ \\ & +\frac{1}{2}\left(-3\varepsilon_1^2\varepsilon_2-\varepsilon_1\varepsilon_2^2-\frac{1}{3}\varepsilon_2^3+\varepsilon_2\varepsilon_6^2\right)C_{266}+\frac{1}{2}\left(-4\varepsilon_1\varepsilon_2\varepsilon_3+\varepsilon_3\varepsilon_6^2\right)C_{366}+\frac{1}{2}\left(\varepsilon_2\varepsilon_4^2+\varepsilon_1\varepsilon_5^2+\varepsilon_4\varepsilon_5\varepsilon_6\right)C_{244} \end{aligned} \tag{2}$$

Table 1. The second-order elastic constants in graphite. The bottom (top) side of the table is referring to the experimental results (theoretical results within LDA density functional theory). The revised experimental elastic constants are shown in the last row of the table.

	Second-order elastic constants C_{ij} (GPa)					
	C_{11}	C_{12}	C_{33}	C_{44}	C_{13}	C_{11}+C_{12}
Trickey *et al* (1992)	--	--	13	--	--	--
Hasegawa *et al* (2004)	--	--	30.4	--	--	--
Yin *et al* (1984)	--	--	54	--	--	--
Boettger *et al* (1996)	--	--	40.8	--	*-0.5*	1279.6
Jansen *et al* (1987)	--	--	56	--	*-12*	1430
Mounet *et al* (2005)	1118	235	29	4.5	-2.8	1353
Blakslee *et al* (1970)	1060±20	180±20	36.5±1	0.018-0.035	15±5	1240±40
Zhao *et al* (1989)	--	--	--	--	22±2	--
Grimsditch (1996)	--	--	--	5.05±0.35	--	--
Rev. Exp. (Cousin *et al* (2003))	1060±20	180±20	36.5±1	5.05±0.35	7.9±3.5	1240±40

Then the elastic constants are determinate by applying different strain components ε_i to the equilibrium lattice configuration. Under strain the primitive lattice vector a_i are transformed into the new lattice vectors a_i' by:

$$\begin{pmatrix} a_1' \\ a_2' \\ a_3' \end{pmatrix} = \begin{pmatrix} a_1 \\ a_2 \\ a_3 \end{pmatrix} \cdot (I + \varepsilon) \tag{3}$$

where ε was the strain tensor and I is the identity matrix. The strain tensor ε is linked with the strain components ε_i by:

$$\varepsilon = \begin{pmatrix} \varepsilon_1 & \frac{1}{2}\varepsilon_6 & \frac{1}{2}\varepsilon_5 \\ \frac{1}{2}\varepsilon_6 & \varepsilon_2 & \frac{1}{2}\varepsilon_4 \\ \frac{1}{2}\varepsilon_5 & \frac{1}{2}\varepsilon_4 & \varepsilon_3 \end{pmatrix} \tag{4}$$

For selected strain components, the respective second-order elastic constants are determined by fitting the strain energy w with the respective energy values obtained by *ab-initio* simulations.

The calculated elastic constants are shown in Table 2 together with the revised experimental elastic constants. This work confirms the previous theoretical studies and in general slightly improves the agreement with respect to the revised experimental data. The elastic constants C_{11}, C_{12}, C_{44} and the value C_{11}+C_{12} are well in agreement with the experiment while the value of C_{33} and in particular, C_{13} show a remarkable difference of about 14% and 129%, respectively. The temperature effects Mounet *et al* (2005) and/or crystal defects El-Barbary *et al* could explain the ±14% difference in values between theory and experiment, nevertheless a disagreement of 129% is far to be explained and a more elaborate explanation should be require. Later in the last section of this work we have shown that the values of the mesoscale elastic constant C_{33}^M and C_{13}^M are both in agreement with experiments within a range ±11%.

The Mesoscale Elastic Theory of Graphene

In this section, we have studied the formation energy of a bent thin plane beyond the harmonic approximation. This theory will describe the mechanical properties of a single layer of graphite, *i.e.* graphene. Within the isotropic elastic theory, the formation energy of a thin bent plane is given by the well know Landau and Lifshitz formula (1986):

$$E_{bent} = \frac{E \cdot h^3}{24\left(1-\sigma^2\right)} \iint \left(\frac{\partial^2 \zeta}{\partial x^2} + \frac{\partial^2 \zeta}{\partial y^2} \right)^2 + 2\left(1-\sigma\right)\left[\left(\frac{\partial^2 \zeta}{\partial x \partial y} \right)^2 - \frac{\partial^2 \zeta}{\partial x^2} \frac{\partial^2 \zeta}{\partial y^2} \right] dxdy \tag{5}$$

where ζ is the vertical displacement of any point on the plane, E is the Young modulus and σ is the Poisson ratio. The simplest solution of the Landau and Lifshitz equation is a pure sinusoidal bending mode along only one direction (for instance, we have chosen the x-direction):

$$\zeta(x, y) = \bar{a} \cdot \sin\left(\frac{2\pi x}{\lambda} \right) \tag{6}$$

where $\bar{a}$ is the amplitude and λ is the wavelength of the bending mode. We have demonstrated[2] that this solution corresponds to the lowest formation energy and therefore it is the fundamental solution of equation 5. Taking in account the latter solution the formation energy of a bent plane became:

$$E_{bent} = \frac{E \cdot h^3}{24\left(1-\sigma^2\right)} \iint \left(\frac{\partial^2 \zeta}{\partial x^2} \right)^2 dx = C_{bent} \frac{\bar{a}^2}{\lambda^3} \qquad \text{where:} \qquad C_{bent} = \frac{\pi^4 \cdot E \cdot h^3 \cdot \Delta y}{3\left(1-\sigma^2\right)} \tag{7}$$

Therefore the most favorable bending mode possesses the largest wavelength λ and the smallest amplitude $\bar{a}$. The relationship between the amplitude $\bar{a}$ and the strain ε is given by the following elliptical integral:

$$\int_0^{\lambda} \sqrt{1 + \left(\frac{\partial \zeta}{\partial x} \right)^2} dx = L_{arc} \quad \rightarrow \quad \int_0^{\lambda} \sqrt{1 + \left(\frac{2\pi \cdot \bar{a}}{\lambda} \cos\left(\frac{2\pi x}{\lambda} \right) \right)^2} dx = L_{arc} \tag{8}$$

where L_{arc} the arc-length of the plane along the x-direction. As this elliptical integral has no analytical solution, we have solved it with numerical approximate solutions. For small value of $\bar{a} / \lambda$ we can expand the square root in Taylor series. Taking until the second order terms the elliptical integral became:

$$\sqrt{1+z^2} = 1 + \frac{z^2}{2} + O\left(z^4\right) \quad \rightarrow \quad \int_0^{\lambda} 1 + \left(\frac{2\pi \cdot \bar{a}}{\lambda} \cos\left(\frac{2\pi x}{\lambda} \right) \right)^2 dx = L_{arc} \quad \rightarrow \quad \bar{a}_{2^{th}} = \frac{L}{\pi} \sqrt{-\varepsilon_{bent}\left(1+\varepsilon\right)} \tag{9}$$

The latter equation represents the 2nd-order approximate solution of the elliptical integral. Taking the n^{th}-order expansion

[2] The general demonstration of this result can be found in Savini *et al*.

of the Taylor series, we have found the respective approximate solution of the elliptical integral $\bar{a}_{n^{th}}$. Test calculations have shown that the 6th-order approximation was a good compromise between precision and calculation time. Here for simplicity we have discussed the results using the simpler 2nd-order approximate solution. Using the 2nd-order approximate solution the formation energy become:

$$E_{bent} = C_{bent}\frac{\bar{a}^2}{\lambda^3} = \frac{C_{bent}}{\pi}\frac{\left(L_{arc}-\lambda\right)}{\lambda^2} \tag{10}$$

In the general case the strain ε applied to the plane should contain two different components:

ε_{bond} : The homogeneous in-plane compression or expansion. In this case, all the distance between atoms lying along the plane are equally compressed or expanded by the same strain amount;

ε_{bend} : The compression due only to the bending with amplitude $\bar{a}$ and wavelength λ. In this case, all the atoms of the plane lie on a sinusoidal surface with the distance between atoms along the plane unchanged.

Therefore, the corresponding bent formation energy can be written as:

$$E_{bent} = \frac{C_{bent}}{\pi}\frac{\left(L_{arc}-\lambda\right)}{\lambda^2} = C_{bent}\frac{-\varepsilon_{bend}}{L\left(1+\varepsilon\right)^2} \tag{11}$$

This simple relation shows that for small deformations the bent formation energy is linearly proportional to the bending strain and inversely proportional to the length of the plate L. Then the total formation energy of the plane is the sum of the bending energy component E_{bend} and the energy due to the homogeneously compression or expansion of the plane E_{bond} :

$$E = E_{bent} + E_{bond} = C_{bent}\frac{-\varepsilon_{bend}}{L\left(1+\varepsilon\right)^2} + C_{11}\varepsilon_{bond}^2 \tag{12}$$

Therefore, in the compressed region we can have the following three scenarios:

1. *Homogeneously compressed flat plane*: In this case, all the atoms lie on the flat plane and the distance between atoms along the *x*-axis are equally compressed. In this regime the formation energy of the graphene plane is:
$$E = C_{11}\cdot\varepsilon^2 \tag{13}$$
2. *Pure uncompressed bent plane*: In this case, all the atoms lie on the flat plane and the distance between atoms along the *x*-axis are equally compressed. In this regime the formation energy of the graphene plane is:
$$E = C_{bent}\cdot\frac{-\varepsilon}{L\left(1+\varepsilon\right)^2} \tag{14}$$
3. *Homogeneously compressed bent plane*: In this case, all the atoms of the plane lie on a sinusoidal surface with the distance between atoms along the *x*-axis equally compressed. In this regime the formation energy lie on the flat plane and the distance between atoms along the *x*-axis are equally compressed. In this regime the formation energy of the graphene plane is:
$$E = E_{bent} + E_{bond} = C_{bent}\frac{-\varepsilon_{bend}}{L\left(1+\varepsilon\right)^2} + C_{11}\varepsilon_{bond}^2 \tag{15}$$

The first and third regimes are shown in the figure 1 (right and left regions, respectively). In the following theorem, we have demonstrated that the second scenario is not possible.

Theorem: A thin plane is always homogeneously compressed (bent or flat), but it is never a purely uncompressed bent plane.

Proof.

Imposing the condition that minimises the total formation energy:

$$\frac{\partial E\left(\varepsilon_{bend}\right)}{\partial\varepsilon_{bend}} = 0 \qquad \text{and} \qquad \frac{\partial^2 E\left(\varepsilon_{bend}\right)}{\partial\varepsilon_{bend}^2} > 0 \tag{16}$$

we found:

$$\varepsilon_{bend} = \varepsilon + \frac{C_{bend}}{2\cdot L\cdot C_{11}\left(1+\varepsilon\right)^2} = \varepsilon + \frac{K}{\left(1+\varepsilon\right)^2} \qquad \text{with} \qquad K = \frac{C_{bend}}{2\cdot L\cdot C_{11}} \tag{17}$$

as the strain component ε_{bend} must be always negative[3] the latter equation represents a solution only when the total strain ε is under a critical value $\varepsilon_{critical}$. The critical strain is found imposing the condition:

[3] A positive value implies imaginary amplitudes with no physical meaning.

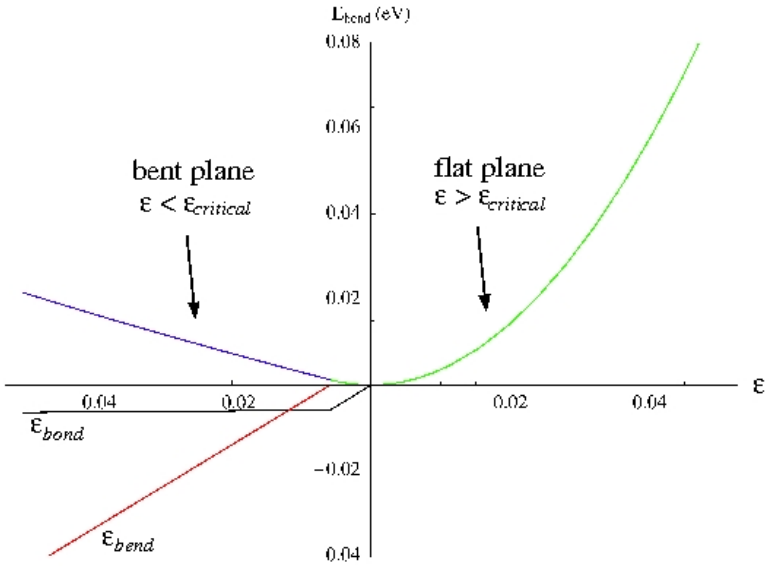

Figure 1. The formation energy of a graphene plane when compressed ($\varepsilon < 0$) or expanded ($\varepsilon > 0$). The green and blue curves represent the formation energies when the strain ε is above or under the critical strain $\varepsilon_{critical}$, respectively. The red line represents the strain component ε_{bend}, while the black line represents ε_{bond} (for simplicity both are shown only in the compression region)

$$\varepsilon_{bend} = 0 \qquad \rightarrow \qquad \varepsilon + \frac{K}{(1+\varepsilon)^2} = 0 \qquad \rightarrow \qquad \varepsilon(1+\varepsilon)^2 + K = 0 \tag{18}$$

imposing a real negative solution, we have found:

$$\varepsilon_{critical} = -\frac{2}{3} + \frac{1}{3}\sqrt[3]{\frac{2}{2-27K+3\sqrt{3}\sqrt{-4K+27K^2}}} + \frac{1}{3}\sqrt[3]{\frac{2-27K+3\sqrt{3}\sqrt{-4K+27K^2}}{2}} \tag{19}$$

Therefore above the critical strain $\varepsilon_{critical}$ the plane are flat ($\varepsilon_{bent} = 0$ and $\varepsilon_{bond} = \varepsilon$), while under the critical strain the plane are bent ($\varepsilon_{bent} = \varepsilon - \varepsilon_{critical}$ and $\varepsilon_{bond} = \varepsilon_{critical}$).

In the following discussion, we have demonstrated that the plane is never a purely uncompressed bent plane. The proof was splits into the two possible cases and demonstrated via *reduction ad absurdum* (in both cases, the contradiction of the proposition is found):

1. Case: $\varepsilon \geq \varepsilon_{critical}$ (*i.e.* flat plane homogeneously compressed or expanded)
   If we suppose that the formation energy of a purely uncompressed bent plane (right sides of the following inequity) is lower than the energy of a homogeneously compressed plane (left sides of the following inequity) we have:

$$C_{11}\varepsilon^2 > C_{bend} \cdot \frac{-\varepsilon}{L(1+\varepsilon)^2} \qquad \rightarrow \qquad \varepsilon^2 > \frac{C_{bend}}{L \cdot C_{11}} \cdot \frac{-\varepsilon}{(1+\varepsilon)^2} \qquad \rightarrow \qquad \varepsilon^2 > -2\varepsilon\frac{K}{(1+\varepsilon)^2} \tag{20}$$

   If we suppose $\varepsilon \geq \varepsilon_{critical}$ the corresponding bent strain is $\varepsilon_{bent} \geq 0$ and we can write the following relations:

$$\varepsilon_{bent} > 0 \qquad \rightarrow \qquad \frac{K}{(1+\varepsilon)^2} > -\varepsilon \tag{21}$$

   Therefore, the inequity of the equation 20 can be written as:

$$\varepsilon^2 > -2\varepsilon\frac{K}{(1+\varepsilon)^2} > 2\varepsilon^2 \qquad \rightarrow \qquad 1 > 2 \tag{22}$$

   The latter inequity is obviously impossible, therefore when $\varepsilon \geq \varepsilon_{critical}$ the plane is always homogeneously compressed or expanded.

2. Case: $\varepsilon \leq \varepsilon_{critical}$ (*i.e.* bent and homogeneously compressed plane)
   If we suppose that exist a range of strain values where the formation energy of a pure uncompressed bent plane (right member of the following inequity) is lower than the energy of a homogeneously compressed bent plane (left member of the following inequity) we have:

$$C_{bend}\cdot\frac{-\varepsilon_{bent}}{L\left(1+\varepsilon\right)^2}+C_{11}\cdot\varepsilon_{bond}^2>C_{bend}\cdot\frac{-\varepsilon}{L\left(1+\varepsilon\right)^2} \tag{23}$$

If we suppose $\varepsilon\le\varepsilon_{critical}$ we have found that the corresponding strain components are:

$$\varepsilon_{bent}=\varepsilon+\frac{K}{\left(1+\varepsilon\right)^2}\qquad\text{and}\qquad\varepsilon_{bond}=\varepsilon-\varepsilon_{bent}=-\frac{K}{\left(1+\varepsilon\right)^2} \tag{24}$$

Therefore the previous inequity became:

$$C_{bent}\frac{-\varepsilon_{bent}}{L\left(1+\varepsilon\right)^2}+C_{11}\frac{K}{L\left(1+\varepsilon\right)^4}+C_{11}\frac{K^2}{\left(1+\varepsilon\right)^4}>C_{bent}\frac{-\varepsilon}{L\left(1+\varepsilon\right)^2}\quad\rightarrow\quad C_{bent}\frac{K}{L\left(1+\varepsilon\right)^4}+C_{11}\frac{K^2}{\left(1+\varepsilon\right)^4}>0$$

$$\rightarrow\quad K^2-\frac{C_{bent}}{L\cdot C_{11}}K>0\quad\rightarrow\quad K^2-2K^2>0\quad\rightarrow\quad -K^2>0 \tag{25}$$

The latter inequity is obviously impossible. Therefore a graphite plane cannot be a purely uncompressed bent plane but it is always homogeneously compressed.

q.e.d.

The Mesoscale Elastic Theory of Graphite

In this section, we have extended the mesoscale elasticity for the graphite case (several graphene planes stacked along the *c*-axis). The main goal of this section is to describe the disregistry energy *i.e.* the interactions between bent planes. Although weak, this energy is of paramount importance in order to describe the full set of the mesoscale elastic constants.

When several graphite planes are bent, we always introduce locally a range of different stacking fault disregistries Δd between the planes. The disregistry Δd is defined with respect to the perfect AB stacking. For nearly flat plane the disregistry Δd is zero while when the slope is negative (positive) the disregistry Δd becomes negative (positive), respectively. As the bending slope is proportional to the amplitude $\bar{a}$ and inversely proportional to the wavelength λ, we can expect that the modulus of the disregistry value $\left|\Delta d\right|$ should be proportional to the ratio $\bar{a}/\lambda$.

A convenient way to find an approximate solution for the disregistry Δd with respect to the amplitude $\bar{a}$, wavelength λ, is to approximate the bending slope with its corresponding tangent line. Within this approximation, the disregistry became:

$$\Delta d\left(\xi\right)=\frac{\pi\cdot\bar{a}\cdot c_0}{\lambda}\cdot\cos\left(\frac{2\pi\cdot\xi}{\lambda}\right)\frac{1}{\sqrt{1+\left[\frac{2\pi\cdot\bar{a}}{\lambda}\cdot\cos\left(\frac{2\pi\cdot\xi}{\lambda}\right)\right]^2}} \tag{26}$$

where $\xi\in\left[0,\lambda\right)$ is the *x*-coordinate along the bent plane.

The latter formula possesses the same periodicity λ of the bended plane. As the $\bar{a}/\lambda$ becomes smaller, the disregistry function tends to a cosine function with amplitude $\left(\pi\cdot\bar{a}\cdot c_0\right)/\lambda$. Then we have studied the formation energies associated with the disregistry $\Delta d(\xi)$ and the strain ε_3 along the *c*-axis. In order to calculate the energy associated with these strain vectors we have applied a grid of 26 displacements along $[1\bar{2}10]$ direction with increments 0.005 ranging from ε_5=0.000 to ε_5=0.125. For each of these displacement we have applied 24 strain ε_3 along [0001] direction with the same increment 0.005 ranging from ε_3=-0.060 to ε_3=0.060.

The corresponding energies of each strained unitcells are calculated using density functional theory within the LDA approximation. Then this energy surface was fitted by a function of order *n*+*m* defined by:

$$E^{fit}\left(\Delta d,\varepsilon_3\right)=\sum_{\alpha=0}^{n}\sum_{\beta=0}^{m}c_{\alpha,\beta}\cdot\left|\sin\left(\frac{\pi}{2}\frac{\Delta d}{a}\right)\right|^{\alpha}\cdot\varepsilon_3^{\beta}\cdot\delta_{\beta=1} \tag{27}$$

this function is an *n*-order power series of sine function along the $[1\bar{2}10]$ direction and an *m*-order polynomial function along the [0001] direction (*c*-axis). The *n*, *m* orders of the function $E^{fit}\left(x,y\right)$ was then increased until the maximum error between fitted values and respective data were equal or less than the precision of the data themselves.

Finally, the total disregistry energy $E^{d}\left(\varepsilon_3,\bar{a},\lambda\right)$ is defined as the sum of the disregistry energy $E^{fit}\left(\Delta d,\varepsilon_3\right)$ over all the atom contributions along the bent plane. Therefore, the total disregistry energy is determined by:

$$E^{fit}\left(\varepsilon_3,\bar{a},\lambda\right)=\sum_{i=1}^{n}E^{fit}\left(\xi_i,\varepsilon_3,\bar{a},\lambda\right) \tag{28}$$

where *n* is how many time the primitive unitcell is repeated along the *x*-axis (*i.e.* the $[1\bar{2}10]$ direction), while ξ_i is the coordinate along the *x*-axis of the i^{th} atom.

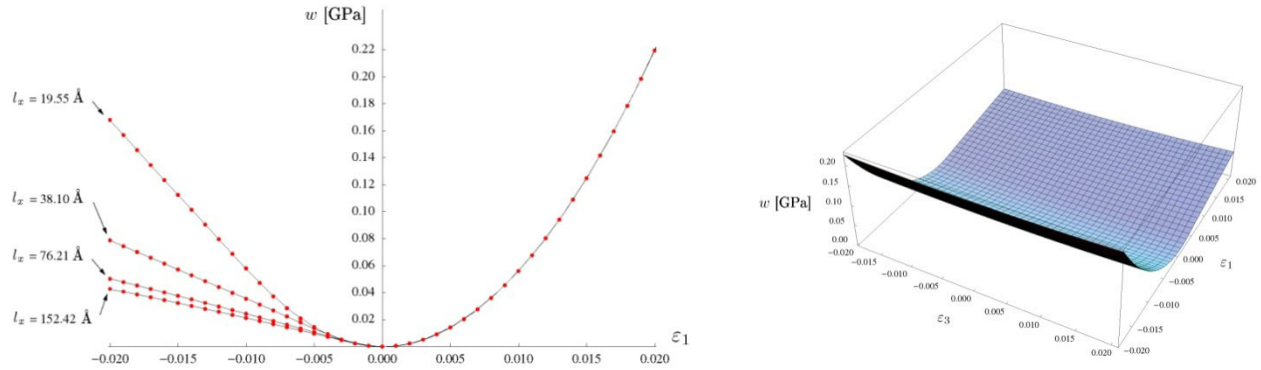

Figure 2. The formation energy per unit volume w with respect to the strain increments ε_1 and/or ε_3. The linear behaviour in the compression region is due to the plane bending. (Left) The mesoscale elastic constant C_{11}^M is determined by fitting the *ab-initio* data; (Right) The corresponding fitted value represents the mesoscale elastic constant C_{13}^M (The unitcell length was 76.21 Å corresponding to 256 numbers of atoms).

Then the respective formation energy of graphite is found by including the energy term due to the disregistry between graphite layers. In analytical formula became:

$$w = \left\{ C_{bend} \cdot \frac{\varepsilon_{critical} - \varepsilon}{L(1+\varepsilon)} + C_{11} \cdot \varepsilon_{critical}^2 + E^d(\varepsilon_3, \bar{a}, \lambda) \right\} \cdot \vartheta(\varepsilon_{critical} - \varepsilon) + C_{11} \cdot \varepsilon^2 \cdot \vartheta(\varepsilon - \varepsilon_{critical}) \tag{29}$$

where C_{11} is the classic elastic constant previously determined (C_{11}=1105 GPa), $E^d(\varepsilon_3, \bar{a}, \lambda)$ is the total disregistry energy and C_{bend} is the bending constant for single plane of graphite (C_{bend} = 254 Pa/Å). The latter formula is used to test and extent the following *ab-initio* methodology. In the density functional approach, we have used different unitcell sizes with number of atoms 64, 128, 256, 512, respectively.

The corresponding lattice vectors $\vec{a}_1, \vec{a}_2, \vec{a}_3$ are orthogonal between each other with length:

$$\begin{cases} l_x = 8 \cdot a_0 \cdot (n_{atoms}/64) \\ l_y = \sqrt{3} \cdot a_0 \\ l_z = c_0 \end{cases} \tag{30}$$

where n_{atoms} is the number of atoms of each unitcell and a_0 is the in-plane lattice constant (a_0 = 2.444 Å).
The mesoscale elastic constants are determined by applying different strain vectors $\vec{\varepsilon}$ to the lattice vectors $\boldsymbol{a}_1$, $\boldsymbol{a}_2$, $\boldsymbol{a}_3$:

$$\begin{pmatrix} \boldsymbol{a}_1 \\ \boldsymbol{a}_2 \\ \boldsymbol{a}_3 \end{pmatrix} = \begin{pmatrix} l_x & 0 & 0 \\ 0 & l_y & 0 \\ 0 & 0 & l_z \end{pmatrix} = \begin{pmatrix} 8 \cdot a_0 \cdot n_{\text{atoms}}/64 & 0 & 0 \\ 0 & \sqrt{3} \cdot a_0 & 0 \\ 0 & 0 & c_0 \end{pmatrix} \tag{31}$$

under strain the primitive vectors $\boldsymbol{a}_{\text{i}}$ are transformed into the new lattice vectors $\boldsymbol{a}_{\text{i}}'$ by:

$$\begin{pmatrix} \boldsymbol{a}_1' \\ \boldsymbol{a}_2' \\ \boldsymbol{a}_3' \end{pmatrix} = \begin{pmatrix} \boldsymbol{a}_1 \\ \boldsymbol{a}_2 \\ \boldsymbol{a}_3 \end{pmatrix} (I + \varepsilon) \tag{32}$$

where I is the identity matrix and ε is the strain tensor:

$$\varepsilon = \begin{pmatrix} \varepsilon_1 & \frac{1}{2}\varepsilon_6 & \frac{1}{2}\varepsilon_5 \\ \frac{1}{2}\varepsilon_6 & \varepsilon_2 & \frac{1}{2}\varepsilon_4 \\ \frac{1}{2}\varepsilon_5 & \frac{1}{2}\varepsilon_4 & \varepsilon_3 \end{pmatrix} \tag{33}$$

the latter tensor is linked to the strain vector by: $\vec{\varepsilon} = (\varepsilon_1, \varepsilon_2, \varepsilon_3, \varepsilon_4, \varepsilon_5, \varepsilon_6)$. The chosen strain components ε_{i} were 41 ranging between ±0.02 with increment 0.001. Then the mesoscale elastic constants were found by fitting the following second-order Lagrangian strain energy:

$$w = +\frac{1}{2}\left(\varepsilon_1^2 + \varepsilon_2^2 + \frac{1}{4}\varepsilon_6^2\right) C_{11}^M + \left(\varepsilon_1\varepsilon_2 - \frac{1}{4}\varepsilon_6^2\right) C_{12}^M + \frac{1}{4}\varepsilon_3^2 C_{33}^M + (\varepsilon_1\varepsilon_3 + \varepsilon_2\varepsilon_3) C_{13}^M + \frac{1}{2}(\varepsilon_4^2 + \varepsilon_5^2) C_{44}^M \tag{34}$$

with respect to the *ab-initio* energies values. For each applied strain, the respective unitcells have been optimised using the conjugate gradient routine implemented in the local density functional approach.

Using the elastic theory and then corroborated with the *ab-initio* results we have found that the critical strain $\varepsilon_{\text{critical}}$ which divides the bent and flat plane behaviours decrease until a fixed wavelength value of ~70 Å (called critical length $\lambda^{critical}$).

Under this critical wavelength, the disregistry energy became dominant freezing the critical strain to a fixed value of 0.0026 for any unitcell longer than $\lambda^{critical}$. The latter property represents the main difference between graphite and graphene mesoscale elastic theory without of which the unambiguous definition of elastic constants it would have been impossible. Indeed due to the frozen critical strain, also the respective mesoscale elastic constants remain fixed for unitcell sizes larger than the critical wavelength. In the following discussion, we have described in details the single mesoscale elastic constants.

Mesoscale Elastic Constants C_{11}^M :

For the mesoscale elastic constants, C_{11}^M the only non-zero strain component is ε_1. In Figure 2 (Left), the *ab-initio* results (red points) are compared with the elastic theory previously developed (black curves). We have found a very good agreement between the two theoretical approaches. The resulting mesoscale elastic constant C_{11}^M drop from 1105 GPa (classical elastic constant, *i.e.* flat plane) to the value 1051 GPa (for unitcell larger than the critical wavelength > 70 Å). Nevertheless, we observed that both the values are in agreement with the experiment (1080±20 GPa). The reason why C_{11}^M does not change appreciably is because the second-order elastic constants are even-order elastic terms. The linear behaviour due to the bending is mainly dominated by the odd-order terms of the Lagrangian energy. Therefore, larger deviation should occur between the third-order mesoscale and classical elastic constants.

Mesoscale Elastic Constants C_{33}^M :

The mesoscale elastic constant C_{33}^M slightly increase from 30.6 GPa (classical elastic constant, *i.e.* flat plane) to the convergent value 31.8 GPa (for unitcell larger that the critical wavelength > 70 Å). This slightly changing is reflecting a weak plane bending when the *c*-axis expands (positive value of the strain ε_3). Compared with the revised elastic constants (36.5±1) the mesoscale elastic constant C_{33}^M is underestimated by 10.4 %.

Mesoscale Elastic Constants C_{13}^M :

In Figure 2 (Right) is shown the strain energy with respect to the strain components ε_1, ε_3. This energy surface is fitted by a 10^{th}-order polynomial function in two variables (ε_1, ε_3). The resulting coefficient term $\varepsilon_1 \times \varepsilon_3$ correspond to the mesoscale elastic constant C_{13}^M . The values found are negative when the plane is flat (above the critical strain) and positive under the critical strain with a convergent value +6.2 GPa (see Table 2). A good agreement with the revised experimental value (7.9 ± 3.5 GPa) is found.

Mesoscale Elastic Constants C_{44}^M :

For the C_{44}^M the only non-zero strain component is ε_5. In this case the *ab-initio* approach showed that the graphite planes are always flat and never bent, therefore the resulting mesoscale elastic constant degenerate into the corresponding classical value $C_{44}^M = C_{44}$.

Table 2. The mesoscale and classical elastic constants compared with the experimental revised elastic constants. Clearly, the mesoscale elastic constants improve the agreement between theory and experimental results (the elastic constants units are in GPa).

	Mesoscale elastic constants [GPa]	Revised elastic constants [GPa]
C_{11}^M	1051	1060 ± 20
C_{12}^M	171	180 ± 20
C_{33}^M	31.8	36.5 ± 1
C_{13}^M	6.2	7.9 ± 3.5
C_{44}^M	4.8	5.05 ± 0.35
$C_{11}^M + C_{12}^M$	1222	1240 ± 40
	Classical elastic constants [GPa]	Revised elastic constants [GPa]
C_{11}	1105	1060 ± 20
C_{12}	182	180 ± 20
C_{33}	30.5	36.5 ± 1
C_{13}	2.3	7.9 ± 3.5
C_{44}	4.8	5.05 ± 0.35
$C_{11} + C_{12}$	1286	1240 ± 40

Mesoscale Elastic Constants C_{12}^M :

Finally, the elastic constant C_{12}^M was found using the following strain components $\vec{\varepsilon} = (\varepsilon_1, \varepsilon_2, 0, 0, 0, 0)$. As for the C_{11}^M case, the corresponding value drop from 182 GPa (classical elastic constant, *i.e.* flat plane) to the value 171 GPa (for unitcell larger that the critical wavelength > 70 Å). We have observed that both are in agreement with the revised experimental value (180 ± 20 GPa).

Conclusion

Summarising we have developed a complete elastic theory beyond the harmonic approximation that describes the behaviour of graphite under any applied strains. We have introduced a new class of elastic constants called mesoscale elastic constants, which confirms with unrivalled precisions the revised experimental elastic constants measured in HOPG samples (see Table 2).

The mesoscale elastic theory predict that under the critical strain the elastic behaviour is due to the classical elastic constants while above the critical strain the elastic behaviour is dominated by the mesoscale elastic constants.

We observe that, different quality of graphite samples could favourite the rising of one elastic behaviour over the other. For instance, non-perfect graphite like HOPG (always polycrystalline materials) should favourite the mesoscale elastic behaviour while single crystal graphite (Kish graphite) should favourite the classical elasticity. Furthermore different experimental measures could be able to detect the mesoscale or classic elasticity depending on the type of the techniques (x-ray, ultrasonic, sonic resonance ort static test methods).

We must observe that the only theoretical value that is not completely in agreement with respect to the experimental data is the mesoscale elastic constant C_{13}^M = 31.8 GPa (the respective revised value is 36.5 ± 1). Nevertheless, the temperature effects Mounet *et al* (2005) and/or crystal defects El-Barbary *et al* can easily explain this relatively small difference (10.4 %) between theory and experiment.

Finally using the same background theory but applied for the graphene case, we can demonstrate (see Savini *et al*):

- The bending modes possess always sinusoidal solutions;
- The 1-dimensional bending is always more favourable than a 2-dimensional one;

The latter results give new insight into the structural atomic properties of 2-dimensional materials with strong implications for the new field of graphene science. Finally, we observe that the mesoscale elastic theory should extend to all the other important layered materials like BN, clays and MgB_2.

Acknowledgements

The authors gratefully acknowledge support from British Energy Generation Ltd. The views expressed in this work do not necessarily represent the views of British Energy Generation Ltd.

References

Al-Barbary, A. A. Heggie, M. I. Telling, R. H. Suarez-Martinez, I. Savini, G. Phys. Rev. Lett. Submitted.
Baker, C. Kelly, A. 1964. Phil. Mag. **9**, 927.
Baskin, Y. Meyer, L. 1955. Physical Review 100, 544.
Blakslee, O. L. Proctor, D. G. Seldin, E. J. Spence, G. B. Weng, T. 1970. Journal of Applied Physics **41**, 3373.
Boettger, J. C. 1996. Phys Rev B 55, 11202.
Cousins, C. S. G. and Heggie, M. I. 2003. Physical Review B **67** 024109.
Dresselhaus, M. S. and Endo M. 2000. Carbon Nanotubes, Springer publishers, Pages 14-16.
Grimsditch, M. 1996. Phys. Status Solidi B 193, K9.
Grimsditch, M. 1983. J. Phys. C 16, L143.
Hasegawa, M. Nishidate K. 2004. Phys Rev B 70, 205431.
Hartwigsen, C. Goedecker, S. Hutter, J. 1998. Phys. Rev. B 58, 3641.
Kelly, B. T. 1981. Physics of Graphite, Applied science publishers.
Jansen, H. J. F. Freeman, A. J. 1987. Phys Rev B 35, 8207.
Landau, L. D. Lifshitz, E. M. 1986. Theory of Elasticity, 3rd edition, vol. 7, Pergamon Press.
Monkhorst, H. J. Pack, J. D. 1976. Phys. Rev. B 13, 5188.
Mounet, N. Marzari, N. 2005. Phys Rev B 71, 205214.
Perdew, J. P. Wang, Y. 1992. Phys. Rev. B 45, 13244.
Savini, G. Heggie M. I. *et al* in preparation.
Trickey, S. B. Muller-Plathe, F. Diercksen, G. H. F. Boettger, J. C. 1992. Phys Rev B 45, 4460.
Yin, M. T. Cohen, M. L. 1984. Phys Rev B 29, 6996.
Zhao, Y. X., Spain I. L. 1989. Phys. Rev. B 40, 993.